JACS
JOURNAL OF THE AMERICAN CHEMICAL SOCIETY

Communication

pubs.acs.org/JACS

Propeller-Shaped Fused Oligothiophenes: A Remarkable Effect of the Topology of Sulfur Atoms on Columnar Stacking

Qi Xiao,[†] Tsuneaki Sakurai,[†,‡] Takahiro Fukino,[†] Kouki Akaike,[§] Yoshihito Honsho,[‡] Akinori Saeki,[‡] Shu Seki,[‡] Kenichi Kato,[∥] Masaki Takata,[∥] and Takuzo Aida*[,†,§]

[†]School of Engineering, The University of Tokyo, 7-3-1 Hongo, Bunkyo-ku, Tokyo 113-8656, Japan

[‡]Graduate School of Engineering, Osaka University, 2-1 Yamadaoka, Suita, Osaka 565-0871, Japan

[§]RIKEN Center for Emergent Matter Science, 2-1 Hirosawa, Wako, Saitama 351-0198, Japan

[∥]RIKEN SPring-8 Center, 1-1-1 Kouto, Sayo-cho, Sayo-gun, Hyogo 679-5148, Japan

Supporting Information

ABSTRACT: Propeller-shaped regioisomers of fused oligothiophenes **F9T$_{endo}$**, **F9T$_{anti}$**, and **F9T$_{exo}$** were successfully synthesized. DFT calculations indicated that their core parts are distorted from planarity due to intramolecular steric repulsions involving large sulfur atoms. In contrast with soft crystalline **F9T$_{anti}$** and **F9T$_{exo}$**, **F9T$_{endo}$** self-assembles into a hexagonal columnar liquid crystal (Col$_h$ LC), displaying a clear X-ray diffraction (XRD) due to its stacked π-conjugated core. In each LC column, well-organized intermolecular S−S contacts are developed triple-helically along the columnar axis with a helical pitch of 4.04 nm. Among LC semiconductors reported to date, Col$_h$ LC **F9T$_{endo}$** displays a top-class charge-carrier mobility (0.18 cm^2 V^{-1} s^{-1}) with a distinct ambipolar character featuring well-balanced hole and electron mobilities. A thin film, prepared by mixing **F9T$_{endo}$** with soluble fullerene PCBM, shows a photovoltaic response, when the fullerene content is large enough to compensate a small absorptivity of **F9T$_{endo}$** for visible light.

With an increasing demand for organic electronics, particular attention has been focused on the development of new π-conjugated organic motifs and their elaborate assembly in the solid state.[1] Promising synthetic strategies along this direction include oxidative fusion of multiple aromatic rings to provide extended π-conjugated disks.[2] Hexabenzocoronene derivatives[3] are representative of such disk-shaped aromatic motifs, where 13 benzene rings are fused two-dimensionally into a large π-conjugated disk. Meanwhile, in view of practical applications to electronic and optoelectronic devices, thiophene derivatives are quite attractive.[4−6] However, reported examples of fused oligothiophene derivatives mostly adopt 2D tape and ribbon-like linear architectures,[7] but their disk-shaped analogues are very limited.[8] Although large thiophene-containing disks have been reported, they are prepared by fusion of triphenylene[9a] and coronene[9b] with thiophenes.

Here we report **F9T$_{endo}$**, **F9T$_{anti}$**, and **F9T$_{exo}$** (Figure 1) whose regioisomeric aromatic cores comprise nine nonlinearly connected fused oligothiophene units. We initially thought that these aromatic cores would adopt a disk shape appropriate for π-

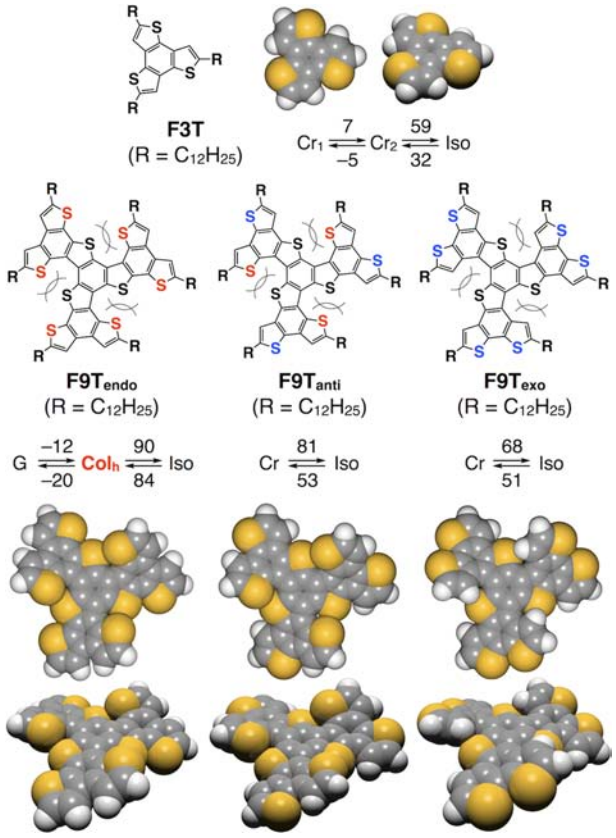

Figure 1. Chemical structures of fused oligothiophenes **F3T**, **F9T$_{endo}$**, **F9T$_{anti}$**, and **F9T$_{exo}$** (R = $C_{12}H_{25}$) together with their computer-generated aromatic core structures (R = H) and phase behaviors with transition temperatures (°C). The core structures were obtained by optimizing their methyl-substituted analogues (R = Me) using the density functional theory (DFT) at the B3LYP/6-31G(d) level. Symbols Cr, Col$_h$, Iso, and G in the phase behaviors denote crystalline, hexagonal columnar (Col$_h$) liquid crystalline, isotropic, and glassy phases, respectively.

Received: September 7, 2013
Published: November 26, 2013

   dx.doi.org/10.1021/ja4092769 | J. Am. Chem. Soc. 2013, 135, 18268−18271

stacking and envisioned that **F9Ts** might self-assemble into columnar liquid crystalline (LC) materials with the help of their six dodecyl side chains. However, to our surprise, only **F9T**$_{endo}$ forms a columnar LC assembly. We then noticed that the aromatic cores of **F9Ts** are not planar but adopt a C_3-symmetric propeller shape due to a considerable steric repulsion among proximal sulfur atoms. In the columnar assembly of **F9T**$_{endo}$, this particular structural feature allows for developing well-organized intermolecular S−S contacts[10] if the stacked cores adopt a helical geometry.[11,12] In this communication, we highlight such unique structural aspects and electronic properties of columnarly assembled **F9T**$_{endo}$.

F9T$_{endo}$, **F9T**$_{anti}$, and **F9T**$_{exo}$ were synthesized via $FeCl_3$-mediated oxidative cyclization of their bithiophene-substituted benzotrithiophene (BTT) precursors.[13] Together with BTT-based **F3T** as a reference (Figure 1),[8] the fused oligothiophenes thus obtained were unambiguously characterized by NMR spectroscopy, MALDI-TOF mass spectrometry, and elemental analysis.[13] Because of their six dodecyl side chains, they are highly soluble in common organic solvents such as hexane, $CHCl_3$, and THF. As described in the introductory part, we initially thought that the fused oligothiophene cores of **F9Ts**, just as the case of **F3T**,[8] adopt a planar conformation. However, structural optimization by DFT calculation (Figure 1) allowed us to notice that they are nonplanar, adopting a propeller shape with a C_3 symmetry. For example, in the case of **F9T**$_{endo}$ and **F9T**$_{anti}$, three congested peripheral areas suffer from a considerably large steric repulsion between two proximal sulfur atoms (Figure 1). Although **F9T**$_{exo}$ does not carry such proximal sulfur atoms, the same issue exists because even small Ar−H hydrogen atoms can sterically conflict with the proximal sulfur atoms. These steric issues do not allow the aromatic cores of **F9Ts** to be planarized.

As shown in Figure 4a (left), the electronic absorption spectra in THF of **F9Ts**, by reference to **F3T** (<306 nm), extend toward a long-wavelength region. Differential pulse voltammetry (DPV) of **F9Ts** in CH_2Cl_2, using $NBu_4^+PF_6^-$ as a supporting electrolyte, gave shallow oxidation potentials as shown in Figure S8 (Supporting Information).[13] Together with the HOMO−LUMO gaps estimated from the red absorption spectral edges, we evaluated the HOMO/LUMO energy levels as −5.6/−1.5 eV for **F3T**, −5.1/−2.0 eV for **F9T**$_{endo}$, −5.2/−2.0 eV for **F9T**$_{anti}$, and −5.3/−2.1 eV for **F9T**$_{exo}$. From these optical and electrochemical band gaps, one may notice that the persistent π-conjugation length of **F9T**$_{endo}$ is slightly but definitely larger than those of the other two **F9Ts**. This is understandable, considering a previous report that α−α connections, involved in fused oligothiophene skeletons, are better for π-electronic conjugation than α−β and β−β connections.[7e,14]

In differential scanning calorimetry (DSC), **F9T**$_{anti}$ and **F9T**$_{exo}$ upon heating only showed a transition from a crystalline phase to an isotropic melt (Figures 1 and S11, Supporting Information).[13] However, **F9T**$_{endo}$, in contrast, displayed a LC mesophase over a wide temperature range from −12 to 90 °C (Figure S11, Supporting Information; from 84 to −20 °C upon cooling).[13] Its crossed polarized optical microscope (POM) image showed a birefringent dendritic texture (Figure 2a) typical of columnar LC materials. In fact, upon exposure to a synchrotron radiation X-ray beam,[15] **F9T**$_{endo}$ in the LC state at 30 °C clearly displayed a set of diffraction peaks at, e.g., q = 2.19, 3.81, and 4.39 nm^{-1} indexed as 100, 110, and 200 planes (Table S1, Supporting Information),[13] respectively, of a hexagonal columnar (Col_h) lattice with a lattice parameter a (intercolumnar distance) of 3.31 nm. Noteworthy, the XRD pattern also displayed a distinct diffraction at q = 17.3 nm^{-1} with a lattice parameter c of 0.364 nm, assignable to the stacking periodicity (Figure 2b). Why does the assembling behavior of **F9T**$_{endo}$ differ from those of the other two regioisomers, despite the fact that no remarkable difference lies in their optical and electrochemical properties? Although this was a puzzling issue for us, we found that **F9T**$_{endo}$ can take full advantage of S−S interactions[10] for columnar stacking. A clue to solve this issue was given by a particular diffraction peak at q = 4.95 nm^{-1} (asterisked in Figure 2b) indicative of the presence of a long-range periodic structure. As described already, the π-stacked columns of **F9T**$_{endo}$ adopt a helical chirality. For the purpose of obtaining a solid support for this geometrical feature, a sheared LC film of **F9T**$_{endo}$ was prepared, whose brightness in POM showed an angle-dependent periodic change (Figure S12, Supporting Information).[13] Furthermore, this sheared LC film, in grazing incidence in-plane X-ray diffraction (GIIXD) analysis (Figure S15, Supporting Information),[13] gave different azimuthal plots for the diffractions indexed as hkl = 001 (Figure 3e) and 100 (Figure 3g), where the former showed two peaks at azimuthal angles (ϕ) = 0 and 180° relative to the sheared direction, whereas the latter exhibited two peaks at ϕ = 90 and 270°. These features allowed us to confirm that the LC columns in the film are oriented along the sheared direction. Then, we examined the azimuthal plots (Figures 3f and S15, Supporting Information) for the asterisked diffraction in Figure 2b, which displayed two split peaks (±20°) centered at ϕ = 0 and 180°. This result demonstrates that the columnar assembly of **F9T**$_{endo}$ adopts a helical geometry along the columnar axis.[12] Taking into account the C_3 symmetry of **F9T**$_{endo}$, the helical pitch of the LC columns can be estimated as 4.04 nm.[16] Since the stacking distance is 0.364 nm (*vide ante*), 11.1 molecules of **F9T**$_{endo}$ are involved in a single pitch. Hence, the dihedral angle of two adjacent core units

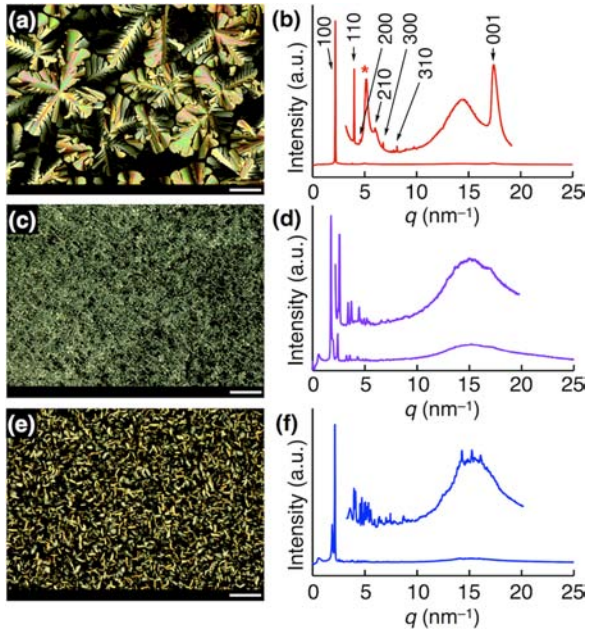

Figure 2. Crossed polarized optical micrographs (POMs) of (a) **F9T**$_{endo}$ at 80 °C, (c) **F9T**$_{anti}$ at 45 °C, and (e) **F9T**$_{exo}$ at 64 °C on cooling from their isotropic melts at a rate of 0.5 °C min^{-1} and subsequent annealing for 2 h. Scale bars indicate 50 μm. X-ray diffraction (XRD) patterns of (b) **F9T**$_{endo}$, (d) **F9T**$_{anti}$, and (f) **F9T**$_{exo}$ at 30 °C after cooling from their isotropic melts at a rate of 1 °C min^{-1} and subsequent annealing for 2 min. The q value for the asterisked diffraction in part b is 4.95 nm^{-1}. For detailed analytical conditions, see the Supporting Information.

dx.doi.org/10.1021/ja4092769 | J. Am. Chem. Soc. 2013, 135, 18268−18271

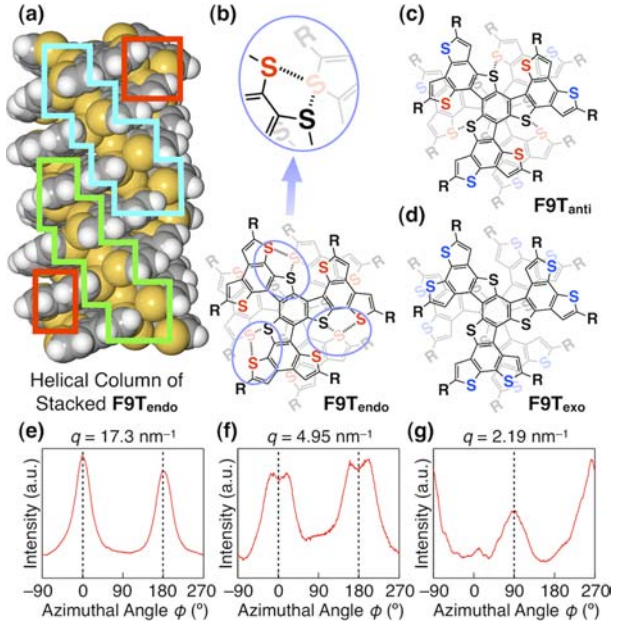

Figure 3. Schematic illustrations of (a) a columnar assembly of **F9T$_{endo}$** via multiple S−S contacts adopting a triple-helical geometry and (b−d) stacked dimer models of (b) **F9T$_{endo}$**, (c) **F9T$_{anti}$**, and (d) **F9T$_{exo}$** with a dihedral angle of 32.5° for investigating the availability of multiple S−S contacts. (e−g) Azimuthal plots for grazing incidence in-plane X-ray diffraction (GIIXD) intensities of a sheared LC film of **F9T$_{endo}$** in regard to the X-ray diffractions at q = (e) 17.3 (hkl = 001), (f) 4.95 (asterisked), and (g) 2.19 (hkl = 100) nm^{-1} in Figure 2b as a function of azimuthal angle (ϕ).

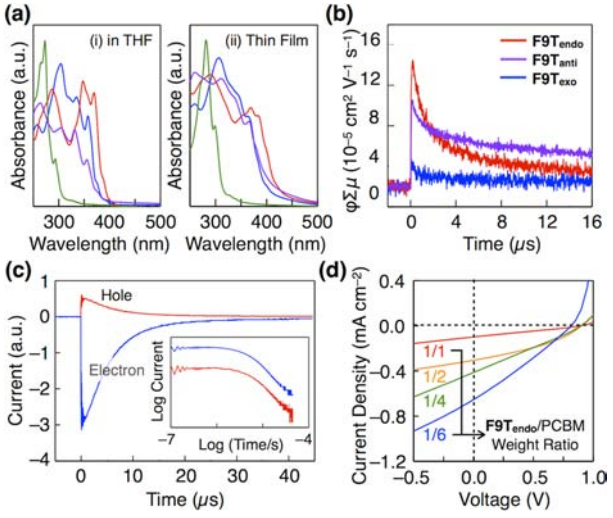

Figure 4. (a) Electronic absorption spectra of THF solutions (left; 1.0 × 10^{-6} M) and spin-coated films (right) of **F3T** (green), **F9T$_{endo}$** (red), **F9T$_{anti}$** (purple), and **F9T$_{exo}$** (blue). (b) FP-TRMC profiles of cast films of **F9T$_{endo}$** (red), **F9T$_{anti}$** (purple), and **F9T$_{exo}$** (blue) at 25 °C upon excitation at 355 nm. (c) Time-of-flight photocurrent transients of **F9T$_{endo}$** for hole (red) and electron (blue) at applied electric fields of +3.3 × 10^4 and −3.3 × 10^4 V cm^{-1}, respectively. The inset shows log−log plots. (d) Current−voltage characteristics of BHJ solar cells using **F9T$_{endo}$**/PCBM blends as active layers at their weight ratios of 1/1 (red), 1/2 (orange), 1/4 (green), and 1/6 (blue).

in a single column is calculated as 32.5°. Thus, in a stacked dimer model of **F9T$_{endo}$** (Figure 3b), if the upper core is positioned with a dihedral angle of 32.5° onto the lower core, three sets of intermolecular S−S contacts are simultaneously made possible. Similar but certainly much weaker S−S contacts are expected for **F9T$_{anti}$** (Figure 3c), whereas no such interactions are available for **F9T$_{exo}$** (Figure 3d). In accord with this consideration, soft-crystalline **F9T$_{anti}$** actually showed a weak diffraction peak at q = 16.7 nm^{-1} (d = 0.376 nm; Figure 2d) assignable to the stacking distance of the core units.

With these structural features, we investigated solid-state electronic properties of **F9T$_{endo}$**, together with those of **F9T$_{anti}$** and **F9T$_{exo}$**. As shown in Figure 4a, their visible-light absorptivities in the solid state are slightly better than those in THF. By means of photoelectron yield spectroscopy (Figure S16, Supporting Information),[13] we evaluated the HOMO energy levels of **F9Ts** in the solid state. Along with the wavelengths for the red absorption spectral edges, their HOMO/LUMO energy levels were evaluated as −5.0/−2.0 eV for **F9T$_{endo}$**, −5.1/−2.0 eV for **F9T$_{anti}$**, and −5.1/−1.9 eV for **F9T$_{exo}$**. The observed energy levels in the solid state are rather close to one another but obviously differ from those of **F3T** (−5.6/−1.6 eV). Next, we investigated their carrier transport properties by means of flash-photolysis time-resolved microwave conductivity (FP-TRMC).[13] FP-TRMC is a method that allows for evaluating short-range (intrinsic) carrier transport properties of materials without electrodes.[17] In this method, a maximum transient conductivity is given by $\varphi\sum\mu_{max}$, where φ and $\sum\mu_{max}$ represent charge carrier generation efficiency and the sum of maximum hole and electron mobilities, respectively. When exposed to a 355 nm laser pulse, drop-cast films of **F9T$_{endo}$**, **F9T$_{anti}$**, and **F9T$_{exo}$** on a quartz plate displayed a transient conductivity with prompt rise and slow decay features (Figure 4b).[13] By taking into account the φ values obtained by the direct-current method (Figure S18, Supporting Information),[17b] charge-carrier mobilities of **F9T$_{endo}$**, **F9T$_{anti}$**, and **F9T$_{exo}$** were evaluated as 0.18, 0.13, and 0.05 cm^2 V^{-1} s^{-1}, respectively. The mobility of 0.18 cm^2 V^{-1} s^{-1} for **F9T$_{endo}$** is one of the largest among those ever reported for LC semiconductors.[11,17a,18] Although soft-crystalline **F9T$_{anti}$** and **F9T$_{exo}$** are both inferior to Col$_h$ LC **F9T$_{endo}$**, the former with a π-stacking profile in XRD (Figures 2d) is better than the latter having no distinct stacking feature (Figure 2f). Being encouraged by the large charge-carrier mobility of **F9T$_{endo}$**, we evaluate its long-range charge-carrier mobility by a time-of-flight technique.[13] Of particular interest, this LC material displayed a distinct ambipolar carrier transport character along with an excellent conducting profile (Figure 4c). For example, at an applied electric field of 3.3 × 10^4 V cm^{-1}, the hole and electron mobilities were 0.02 and 0.03 cm^2 V^{-1} s^{-1}, respectively, and well balanced (Figure S19, Supporting Information).[13]

These observations prompted us to investigate whether **F9T$_{endo}$**, in combination with a soluble fullerene (phenyl C$_{61}$ butyric acid methyl ester; PCBM), is usable as an active layer for a bulk-heterojunction organic photovoltaic (OPV) cell. Most likely due to an intrinsically small absorptivity of **F9T$_{endo}$** for visible light (*vide ante*), the power conversion efficiency (PCE) at an **F9T$_{endo}$**/PCBM ratio of, e.g., 1/1 (w/w), was only 0.023% (Figure 4d). However, by increasing the content of visible-light absorbing PCBM, the efficiency was improved to some extent, where a PCE value of 0.15% was obtained at an **F9T$_{endo}$**/PCBM ratio of 1/6 (w/w).[19] This result encourages further studies to enhance the visible-light absorptivity of the LC material.

In conclusion, we developed a new family of fused oligothiophenes **F9Ts** (Figure 1), which adopt a C_3-symmetric propeller geometry. **F9T$_{endo}$** self-assembles into a hexagonal

dx.doi.org/10.1021/ja4092769 | J. Am. Chem. Soc. 2013, 135, 18268−18271

columnar LC mesophase over a wide temperature range including room temperature. Its LC columns are constructed by well-organized intermolecular S−S contacts that develop triple-helically along the columnar axis with a pitch of 4.04 nm (Figure 3). So far, S−S interactions have mostly been utilized for enhancing the 2D structural integrity of crystalline materials but are much less explored for the formation of columnarly assembled π-conjugated motifs.[10b] Among LC semiconductors reported to date, **F9T$_{endo}$** shows a top-class charge-carrier mobility with a well-balanced ambipolar character (Figure 4). Structural elaboration of **F9T$_{endo}$** to enhance its visible-light absorptivity is one of the interesting subjects worthy of further investigation.

■ ASSOCIATED CONTENT

Supporting Information

Details of synthesis and characterization of **F3T** and **F9Ts**, NMR, POM, XRD, electrochemical, and electrical data, and results of computational simulations. This material is available free of charge via the Internet at http://pubs.acs.org.

■ AUTHOR INFORMATION

Corresponding Author

aida@macro.t.u-tokyo.ac.jp

Notes

The authors declare no competing financial interest.

■ ACKNOWLEDGMENTS

Synchrotron radiation experiments were performed at BL44B2[15] in SPring-8 with the approval of RIKEN (Proposal No. 20100067). Q.X. thanks the Ministry of Education, Culture, Sports, Science and Technology, Japan, for financial support (No. 082158). T.S. and T.F. thank the Japan Society for the Promotion of Science for a Young Scientist Fellowship.

■ REFERENCES

(1) (a) Li, Q., Ed. *Self-Organized Organic Semiconductors: From Materials to Device Applications*; John Wiley & Sons: Hoboken, NJ, 2011. (b) Nakanishi, T., Ed. *Supramolecular Soft Matter: Applications in Materials and Organic Electronics*; John Wiley & Sons: Hoboken, NJ, 2011.

(2) (a) Sarhan, A. A. O.; Bolm, C. *Chem. Soc. Rev.* **2009**, *38*, 2730−2744. (b) Wu, W.; Liu, Y.; Zhu, D. *Chem. Soc. Rev.* **2010**, *39*, 1489−1502. (c) Myśliwiec, D.; Donnio, B.; Chmielewski, P. J.; Heinrich, B.; Stepien, M. *J. Am. Chem. Soc.* **2012**, *134*, 4822−4833.

(3) For hexabenzocoronene derivatives: (a) Wu, J.; Pisula, W.; Müllen, K. *Chem. Rev.* **2007**, *107*, 718−747. (b) Fukushima, T.; Aida, T. *Philos. Trans. R. Soc., A* **2007**, *365*, 1539−1552. (c) Pisula, W.; Feng, X.; Müllen, K. *Adv. Mater.* **2010**, *22*, 3634−3649.

(4) For extended π-conjugated thiophene derivatives: (a) Mccullough, R. D. *Adv. Mater.* **1998**, *10*, 93−116. (b) Osaka, I.; Mccullough, R. D. *Acc. Chem. Res.* **2008**, *41*, 1202−1214. (c) Mishra, A.; Ma, C.-Q.; Bauerle, P. *Chem. Rev.* **2009**, *109*, 1141−1276.

(5) For thiophene-containing low band gap copolymers: (a) Bundgaard, E.; Krebs, F. C. *Macromolecules* **2006**, *39*, 2823−2831. (b) Zhou, H.; Yang, L.; You, W. *Macromolecules* **2012**, *45*, 607−632.

(6) For thiophene-based liquid crystals: (a) Funahashi, M.; Hanna, J. *Adv. Mater.* **2005**, *17*, 594−598. (b) Yasuda, T.; Ooi, H.; Morita, J.; Akama, Y.; Minoura, K.; Funahashi, M.; Shimomuro, T.; Kato, T. *Adv. Funct. Mater.* **2009**, *19*, 411−419.

(7) For fused oligothiophenes: (a) Xiao, K.; Liu, Y.; Qi, T.; Zhang, W.; Wang, F.; Gao, J.; Qiu, W.; Ma, Y.; Cui, G.; Chen, S.; Zhan, X.; Yu, G.; Qin, J.; Hu, W.; Zhu, D. *J. Am. Chem. Soc.* **2005**, *127*, 13281−13286. (b) Takimiya, K.; Ebata, H.; Sakamoto, K.; Izawa, T.; Otsubo, T.; Kunugi, Y. *J. Am. Chem. Soc.* **2006**, *128*, 12604−12605. (c) Zhou, Y.; Liu, W.-J.; Ma, Y.; Wang, H.; Qi, L.; Cao, Y.; Wang, J.; Pei, J. *J. Am. Chem. Soc.* **2007**, *129*, 12386−12387. (d) Okamoto, T.; Kudoh, K.; Wakamiya, A.; Yamaguchi, S. *Chem.—Eur. J.* **2007**, *13*, 548−556. (e) Brusso, J. L.; Hirst, O. D.; Dadvand, A.; Ganesan, S.; Cicoira, F.; Robertson, C. M.; Oakley, R. T.; Rosei, F.; Perepichkat, D. F. *Chem. Mater.* **2008**, *20*, 2484−2494.

(8) For benzotrithiophene derivatives: (a) Nicolas, Y.; Blanchard, P.; Levillain, E.; Allain, M.; Mercier, N.; Roncali, J. *Org. Lett.* **2004**, *6*, 273−276. (b) Guo, X.; Wang, S.; Enkelmann, V.; Baumgarten, M.; Müllen, K. *Org. Lett.* **2011**, *13*, 6062−6065. (c) Nielsen, C. B.; Fraser, J. M.; Schroeder, B. C.; Du, J.; White, A. J. P.; Zhang, W.; McCulloch, I. *Org. Lett.* **2011**, *13*, 2414−2417.

(9) (a) Luo, J.; Zhao, B. M.; Chan, H. S. O.; Chi, C. Y. *J. Mater. Chem.* **2010**, *20*, 1932−1941. (b) Chen, L.; Punireddi, S. R.; Tan, Y.-Z.; Baumgarten, M.; Zschieshang, U.; Enkelmann, V.; Pisula, W.; Feng, X.; Klauk, H.; Müllen, K. *J. Am. Chem. Soc.* **2012**, *134*, 17869−17872.

(10) For crystals containing defined S−S contacts: (a) Rowland, R. S.; Taylor, R. *J. Phys. Chem.* **1996**, *100*, 7384−7391. (b) Werz, D. B.; Gleiter, R.; Rominger, F. *J. Am. Chem. Soc.* **2002**, *124*, 10638−10639. (c) Kobayashi, K.; Masu, H.; Shuto, A.; Yamaguchi, K. *Chem. Mater.* **2005**, *17*, 6666−6673. (d) Bleiholder, C.; Werz, D. B.; Köppel, H.; Gleiter, R. *J. Am. Chem. Soc.* **2006**, *128*, 2666−2674.

(11) For sulfur-containing helical columnar LCs: Adam, D.; Schuhmacher, P.; Simmerer, J.; Häussling, L.; Siemensmeyer, K.; Etzbach, K. H.; Ringsdorf, H.; Haarer, D. *Nature* **1994**, *371*, 141−143.

(12) For helical columnar LCs without sulfur atoms: (a) Pisula, W.; Tomović, Z.; Watson, M. D.; Müllen, K.; Kussmann, J.; Ochsenfeld, C.; Metzroth, T.; Gauss, J. *J. Phys. Chem. B* **2007**, *111*, 7481−7487. (b) Hayashi, H.; Nihashi, W.; Umeyama, T.; Matano, Y.; Seki, S.; Shimizu, Y.; Imahori, H. *J. Am. Chem. Soc.* **2011**, *133*, 10736−10739. (c) Percec, V.; Sun, H. -J.; Leowanawat, P.; Peterca, M.; Graf, R.; Spiess, H. W.; Zeng, X.; Ungar, G.; Heiney, P. A. *J. Am. Chem. Soc.* **2013**, *135*, 4129−4148.

(13) See the Supporting Information.

(14) Ma, C.-Q.; Mena-Osteritz, E.; Debaerdemaeker, T.; Wienk, M. M.; Janssen, R. A. J.; Bäuerle, P. *Angew. Chem., Int. Ed.* **2007**, *46*, 1679−1683.

(15) Kato, K.; Hirose, R.; Takemoto, M.; Ha, S.; Kim, J.; Higuchi, M.; Matsuda, R.; Kitagawa, S.; Takata, M. *AIP Conf. Proc.* **2010**, *1234*, 875−878.

(16) The pitch (P) of the triple-helical strand of LC Col$_h$ **F9T$_{endo}$** was estimated by the following equation: $P/3 = d^*/\cos \Delta\phi$, where d^* and $\Delta\phi$ were 1.27 nm and 20°, respectively. For the helical diffraction theory, see: (a) Cochran, W.; Crick, F. H. C.; Vand, V. *Acta Crystallogr.* **1952**, *5*, 581−586. (b) Percec, V.; Won, B.; Peterca, M.; Heiney, P. A. *J. Am. Chem. Soc.* **2007**, *129*, 11265−11278.

(17) (a) Saeki, A.; Koizumi, Y.; Aida, T.; Seki, S. *Acc. Chem. Res.* **2012**, *45*, 1193−1202. (b) Yasutani, Y.; Saeki, A.; Fukumatsu, T.; Koizumi, Y.; Seki, S. *Chem. Lett.* **2013**, *42*, 19−21.

(18) For LC semiconductors with excellent charge-carrier mobilities: (a) Funahashi, M.; Zhang, F.; Tamaoki, N. *Adv. Mater.* **2007**, *19*, 353−358. (b) Iino, H.; Takayashiki, Y.; Hanna, J.; Bushby, R. J.; Haarer, D. *Appl. Phys. Lett.* **2005**, *87*, 192105. (c) Sakurai, T.; Shi, K.; Sato, H.; Tashiro, K.; Osuka, A.; Saeki, A.; Seki, S.; Tagawa, S.; Sasaki, S.; Masunaga, H.; Osaka, K.; Takata, M.; Aida, T. *J. Am. Chem. Soc.* **2008**, *130*, 13812−13813. (d) Feng, X.; Marcon, V.; Pisula, W.; Hansen, M. R.; Kirkpatrick, J.; Grozema, F.; Andrienko, D.; Kremer, K.; Müllen, K. *Nat. Mater.* **2009**, *8*, 421−426.

(19) An OPV device composed of **F9T$_{endo}$**/PCBM (1/6 w/w) showed J_{SC} = 0.65 mA cm^{-2}, V_{OC} = 0.81 V, FF = 0.27, and η (PCE) = 0.15% (Figure 4d).